Acta Cryst. (1999). B**55**, 448–458

Phase-transition-induced twinning in the 1:1 adduct of hexamethylenetetramine and azelaic acid

Marc Hostettler,* Henrik Birkedal, Manuel Gardon, Gervais Chapuis, Dieter Schwarzenbach and Michel Bonin

Institute of Crystallography, University of Lausanne, BSP Dorigny, CH-1015 Lausanne, Switzerland.
E-mail: marc.hostettler@ic.unil.ch

(*Received 20 October 1998; accepted 10 December 1998*)

Abstract

The title compound, $C_6H_{12}N_4{\cdot}C_9H_{16}O_4$, undergoes several thermotropic phase transitions. The crystalline structure is layered, with sheets of azelaic acid linked to sheets of hexamethylenetetramine by hydrogen bonds. In the room-temperature phase, the azelaic acid molecules are disordered. By lowering the temperature, this disorder partially disappears. The ordering is clearly observed in reciprocal space where on the rods of diffuse scattering, present in the room-temperature phase, a series of superstructure reflections emerges. This phase transition leads to twin-lattice quasi-symmetry (TLQS) twinning. The structure of this twinned phase is explored in this paper. There are two orientational domains linked by a mirror plane which relates disordered orientations of the acid molecules above the phase transition. A single domain has space group $P2_1/c$. The structure has been solved and refined on the complete set of data to $R_1 = 0.0469$. The chains remain partially disordered, showing two acid groups with unequal population: the major form corresponding to a carboxylic acid and the minor to a carboxylate. The ordering of the structure, when going through the phase transition, is interpreted in terms of stabilization by C—H$\cdots$O hydrogen bonding. A least-squares estimator of the twinning volume ratio is developed that gives an expression for the twinning ratio in terms of the intensities of nonoverlapping reflections. The twinning ratio obtained in the structure refinement compares very well with that obtained from this estimator.

1. Introduction

The 1:1 adduct (HMTA) of hexamethylenetetramine, $C_6H_{12}N_4$, and azelaic acid, $C_9H_{16}O_4$, belongs to a series of compounds forming layer structures with sheets of hexamethylenetetramine (HMT) alternating with sheets of the alkanedioic acid, $HOOC(CH_2)_{n-2}COOH$. Hydrogen bonds between the carboxylic acid groups and the N atoms in HMT provide the links between the layers. It appears that the structures can be divided into two categories at ambient pressure, depending on the parity of n: for n even the structures exhibit incommensurate phases, and for n odd the compounds show disordered and/or twinned phases. At present two structures with n even have been described: HMT with suberic acid, $n = 8$ (Bussien Gaillard *et al.*, 1996), and HMT with sebacic acid, $n = 10$ (Bussien Gaillard *et al.*, 1998). Both of these show strong anharmonic modulation at room temperature. They undergo lock-in phase transitions at $T = 123$ K and 291 K for the suberic and sebacic acid adducts, respectively (Bonin & Gardon, 1999). For n odd, structural studies have only been reported for HMTA, $n = 9$, until now. In another paper (Gardon *et al.*, 1999), we have presented the temperature phase diagram (see Fig. 1) and the structure of the room-temperature phase.

In HMTA, four solid phases have been identified. The nature of the high-temperature phase (phase I) just below fusion is presently unknown as the experiments performed were inconclusive. It was determined that it is not crystalline. The room-temperature phase (phase II) is orthorhombic and disordered. The cell parameters are $a = 9.422$ (1), $b = 7.199$ (1), $c = 26.131$ (4) Å, the space group being *Cmcm*. The diffractograms of phase II show rods of diffuse scattering along **a***. This structure was solved using only the Bragg reflections. The HMT

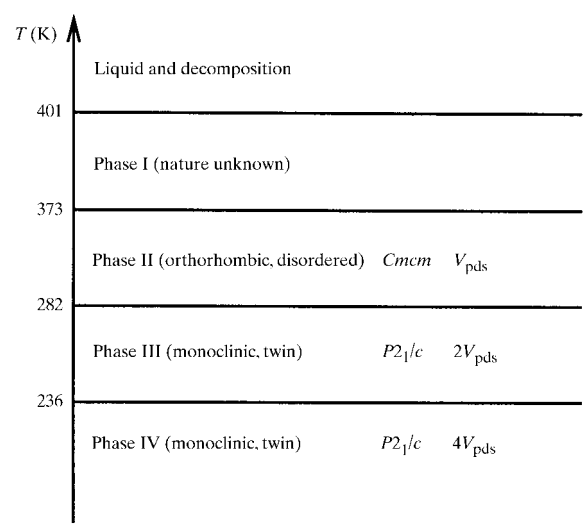

Fig. 1. Phase diagram established by differential scanning calorimetry and diffraction methods. V_{pds} is the volume of the primitive diamond-shaped unit cell of phase II.

molecules are ordered while the chains are disordered. There are two symmetry-related conformations of the carbon chain but the carboxylic acid groups assume more than two orientations. A model describing the diffuse scattering in terms of small ordered domains with varying correlation lengths was established. This model was used to simulate the observed rods of diffuse scattering, for which good qualitative agreement was obtained (Gardon *et al*., 1999).

In the present paper, we discuss the first low-temperature phase, phase III. The structure of the last low-temperature phase, phase IV, will be published in a forthcoming paper (Birkedal *et al*., 1999). Instead of the *C*-centred orthorhombic cell, a primitive diamond-shaped cell can be chosen for phase II, with dimensions a = 5.929, b = 26.131 Å, $c = a$ and β = 105.24°. The volume of this unit cell is referred to as V_{pds} in Fig. 1. At the phase transition II→III, V_{pds} doubles and the symmetry goes from orthorhombic to monoclinic. The diffuse lines, present in phase II, disappear below the transition temperature, showing an essential ordering of the structure. At their place superstructure reflections appear. The phase transition leads to TLQS twinning (Giacovazzo, 1992) with two orientational domains. Each superstructure reflection belongs to a single domain while reflections corresponding to the Bragg peaks of phase II are superpositions of reflections from both domains. We start by discussing the identification and classification of twinning phenomena in phase III. Then we treat the general problem of estimating the volume ratios in TLQS twins. We show that the volume ratio calculated through the ratio of the sums of the intensities of nonoverlapping reflections is a least-squares estimate with a particular choice of weights. The structure solution and refinement using all reflections is then described. The value of the twinning ratio from the refinement is found to be in good agreement with that calculated from the nonoverlapping reflections. Finally, the packing of the structure and the link between twinning and structural characteristics are discussed.

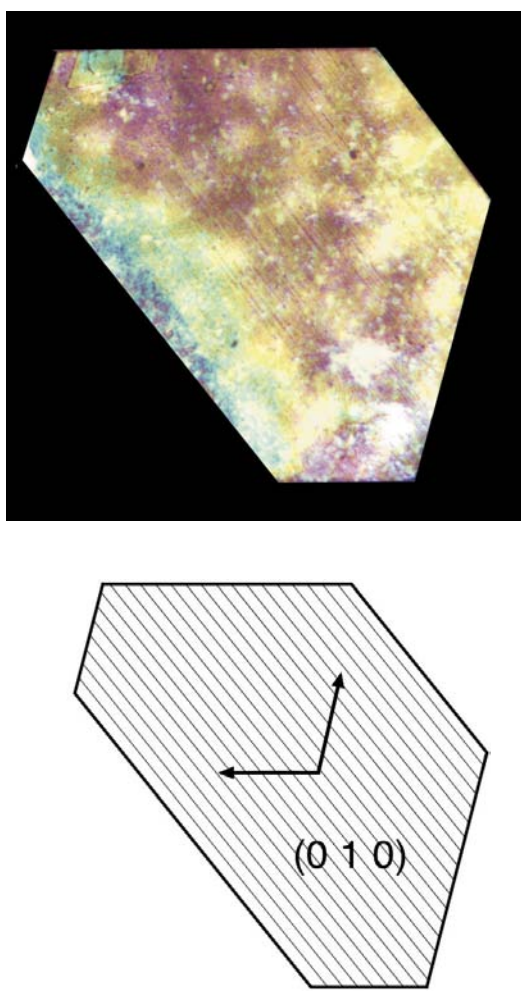

Fig. 2. Top: orthoscopic study of HMTA phase III. The twin domains are clearly revealed through the presence of lines parallel to the natural face of the crystal. Temperature ~273 K. Bottom: schematic representation of the observed domain pattern. The axes shown are **a** and **c** of the primitive diamond-shaped cell of the orthorhombic phase II.

2. Experimental

2.1. *Crystallization*

HMT was mixed with an equimolar amount of azelaic acid in ethanol, which was subsequently evaporated leaving a white powder. This raw product was recrystallized by slow evaporation from acetonitrile, yielding single crystals of suitable quality for X-ray diffraction studies. The crystals are generally of higher quality if the recrystallization is performed at lower temperatures (~278–283 K).

2.2. *Optical studies*

Orthoscopic studies were performed by means of an M8 binocular (×50) from Wild Heerbrugg between crossed Nicols polarizers. The crystals were cooled with a flow of cold nitrogen gas, allowing a lowest sample temperature of 273 K to be reached.

2.3. *X-ray diffraction*

Single-crystal X-ray diffraction data were collected at 258 K. The temperature was controlled using a nitrogen gas stream. A Stoe image-plate diffractometer (IPDS) using graphite monochromated Mo $K\alpha$ radiation was used. The data were collected with the oscillation method, $0 \leq \varphi \leq 359°$, $\Delta\varphi = 1°$. The raw frames were reduced to Bragg intensities using the Stoe IPDS software (Stoe, 1997). Data reduction was carried out in a monoclinic supercell, a_s = 11.7813 (14), b_s = 26.071 (2), c_s

Table 1. *Averaging statistics for the three reflection classes*

*D*1 and *D*2 stand for domain 1 and domain 2, respectively. $\langle I/\sigma(I)\rangle$ is calculated for the averaged data.

Reflection class	h_s	l_s	No. measured	No. unique	$R_{\rm int}$	$\langle I/\sigma(I)\rangle$
Common reflections	$2n$	$2n$	2766	649	0.0570	26.86
Superstructure, *D*1	$2n$	$2n+1$	2543	582	0.0547	16.81
Superstructure, *D*2	$2n+1$	$2n$	947	212	0.3677	6.21

= 11.8868 (11) Å, and β_s = 106.118 (9)°, which permits the reflections from both domains to be simultaneously indexed (Fig. 3).

3. Identification of twinning phenomena

3.1. *Optical studies*

A direct observation of twinning can be made from an orthoscopic study provided that the optical indicatrix is not uniaxial and that the domains are macroscopic in size. In Fig. 2, the orthoscopic pattern of phase III is shown. The crystals are clearly birefringent. The phase transition II→III is associated with the appearance of a family of dark lines in the optical interference pattern. Systematically we observed only one type of line, each parallel to the natural face $(10\bar{1})$ of phase II indexed in the primitive diamond-shaped cell. This pattern can be explained by two orientational domains separated by domain walls. This confirms the change of crystal system occurring during the phase transition.

Note that, within the resolution of the optical studies, no domain walls were observed parallel to (101).

3.2. *X-ray diffraction*

The twinning phenomena can also be identified on diffractograms. A comparison of the (*h*4*l*) layer at T = 285 K (phase II) and at T = 258 K (phase III) is given in Fig. 3. These images were obtained by a reconstruction of reciprocal layers from the oscillation frames of the data collections using the program *SPACE* of the Stoe software package (Stoe, 1997). Holes appear in the reconstructed layers because the data collections did not cover 360° in φ† and because of the well known blind regions inherent in the oscillation method.

Phase III exhibits two types of reflections. The main reflections, circles in Fig. 3, are common to both domains. They correspond to the Bragg reflections of phase II. The superstructure reflections emerging from the diffuse lines lead to a change in the unit cell. The complete diffraction pattern of phase III can be indexed in a supercell corresponding to a doubling of **a** and **c** of the primitive diamond-shaped cell of phase II. However, this setting is associated with extinction rules typical for twinned crystals, leading us to consider the formation of two orientational domains. This is consistent with the observation (Fig. 2) of domain walls. Thus, only one lattice constant, **c**, is doubled.‡ The domains are linked by a mirror plane parallel to $(10\bar{1})$ of the supercell (see Fig. 2). This mirror plane is one of the two lost in the transition from orthorhombic to monoclinic symmetry. Alternatively, one can choose to consider the other mirror plane, parallel to (101) of the supercell, as the twinning operation. These descriptions are equivalent. When indexed in the monoclinic cell of domain 1, $(10\bar{1})$ of the supercell corresponds to $(20\bar{1})$.

From the extinction rules of the diffractograms associated with one domain, the space group was unambiguously determined as $P2_1/c$.

The reconstructed layers and the intensities observed on the raw frames clearly show that one twin component dominates, as evidenced by much stronger superstructure reflections of the one compared to the other. The predominant domain is referred to as domain 1. Supercell index conditions for the three classes of reflections, common reflections, superstructure reflections of domain 1, and superstructure reflections of domain 2, are given in Table 1.

3.3. *Classification of twinning type*

Let us define the phases adjacent to the II→III transition as G (*Cmcm*) and H ($P2_1/c$). Furthermore, let $|G|$, $|H|$, V_G and V_H be the orders of the point groups and the volumes of the primitive unit cells. The possible number, n, of types of single-domain states is given as (Aizu, 1970; Wadhawan, 1997)

$$n = \frac{|G|}{|H|}\frac{V_H}{V_G}. \qquad (1)$$

Presently we have $|G|$ = 8, $|H|$ = 4, $V_G = V_{\rm pds}$ and $V_H = 2V_{\rm pds}$, leading to n = 4. This corresponds to two possible single-domain states from the two mirror planes lost in the transition. In HMTA we observe only one type of domain wall. The reason for this can be found in the intermolecular interactions in the crystal (see below).

The twinning is by TLQS (Giacovazzo, 1992). According to the tensor classification of Wadhawan (1997), phase III can be further characterized as an *S* twin, *i.e.* arising from a ferroelastic phase transition. For this class of twinning the orientational domains differ in all second-rank macroscopic tensor properties, such as the spontaneous strain tensor, the dielectric tensor, the

† For phase II 200° were covered in φ, while for phase III the coverage was 359°.

‡ Note that the choice of doubled lattice constant is arbitrary; **a** could equally well have been chosen.

magnetic permeability tensor, *etc*. For phase III, this is confirmed by a change in the orientation of the optical indicatrix across the domain walls as described in §3.1.

4. Twinning ratio

The twinning volume ratio is a refinable parameter in the structure refinement by least squares (Jameson, 1982). In cases in which nonoverlapping reflections are present, it can also be estimated from the intensities of these reflections. Typically, the intensity ratio between two domains is estimated as the ratio of the sums of the intensities of a set of corresponding nonoverlapping reflections measured in both domains. In the following it is shown that the least-squares estimate of the intensity ratio is indeed equal to the ratio of the sum of the intensities provided that a special choice of weights is made. The general problem of scaling different data sets has been treated by Hamilton *et al*. (1965) and further developed by Sparks (1970). Their method is focused on the extraction of the average intensity of several measurements by the definition of scale ratios between different data sets. It is based on an iterative nonlinear least-squares approach. In the present work, we are mainly interested in obtaining an estimator of the scaling factors without derivation of an average intensity. This leads to the new development described below. Let us consider the general case of a twin consisting of D domains where nonoverlapping reflections are present. Consider further a reflection from a single domain i. The intensity of this reflection is written $I_{i,n}$, where n defines the reflection. Let $I_{0,n}$ be the true intensity of reflection n in a monodomain structure. Then

$$I_{i,n} \simeq k_i I_{0,n} \quad \text{for } i = 1, D. \tag{2}$$

Following Hamilton *et al*. (1965), the least-squares residual to be minimized is

$$R_w = \sum_{i=1}^{D} \sum_{n=1}^{N} w_{i,n}(I_{i,n} - k_i I_{0,n})^2. \tag{3}$$

Assuming that the weights of the observations are based on inverse variances from counting statistics and applying (2) yields

$$w_{i,n} = [\sigma^2(I_{i,n})]^{-1} = I_{i,n}^{-1} \simeq (k_i I_{0,n})^{-1}. \tag{4}$$

Setting the first derivatives of R_w with respect to k_i to zero, introducing scale ratios $\kappa_{ij} = k_i/k_j$, and using these weights leads to

$$\kappa_{ij} = \sum_{n=1}^{N} I_{i,n} \Big/ \sum_{n=1}^{N} I_{j,n}. \tag{5}$$

Thus with this special choice of weights, the least-squares estimate corresponds to the intuitive definition of scale ratios. Deriving the standard uncertainty (s.u.) using simple error propagation based on (5) leads to

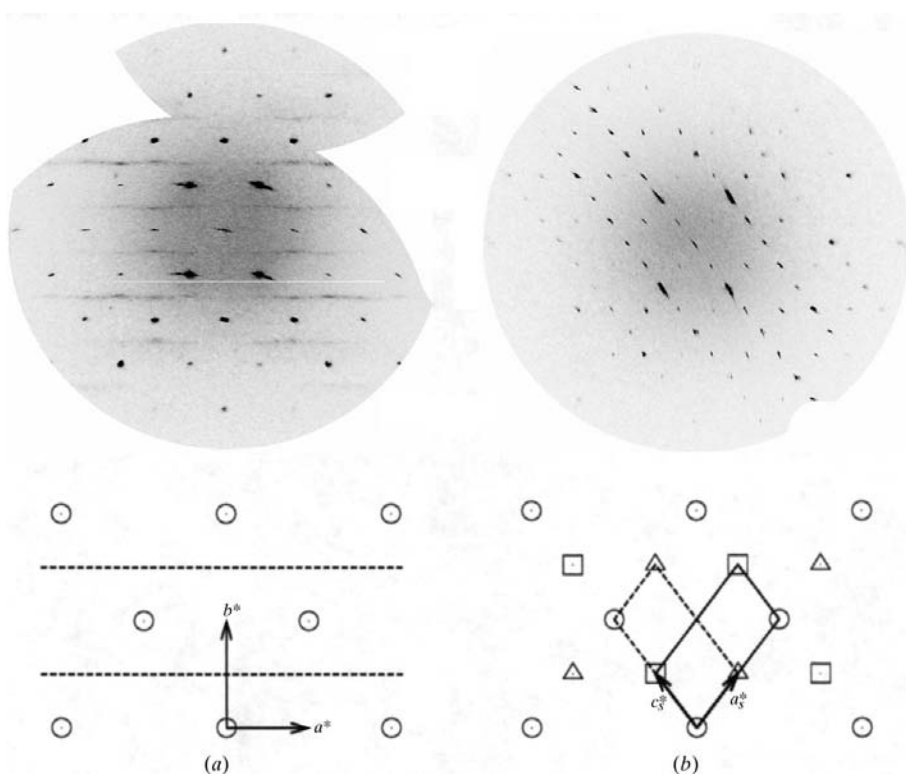

Fig. 3. Corresponding layers of reciprocal space for HMTA phases II and III. Top: reconstructed layers. Bottom: schematic representations. (*a*) Phase II at 285 K. Note the lines of diffuse scattering (dashed lines in the schematic drawing). The unit cell of the centred orthorhombic lattice of phase II is indicated; the layer has indices (*hk*4). (*b*) Phase III at 258 K. Note the presence of superstructure reflections. The axes are those of the supercell (see text). The superstructure reflections are drawn as squares and triangles for domains 1 and 2, respectively. The monoclinic unit cells are drawn with full lines for domain 1 and dashed lines for domain 2. The layer is (*h*4*l*).

Table 2. *Experimental details*

Crystal data	
Chemical formula	$C_6H_{12}N_4{\cdot}C_9H_{16}O_4$
Chemical formula weight	328.41
Cell setting	Monoclinic
Space group	$P2_1/c$
Temperature (K)	258 (1)
a (Å)	5.8907 (7)
b (Å)	26.071 (2)
c (Å)	11.8868 (11) $\simeq 2a$ (11.7814)
β (°)	106.118 (9)
V (Å^3)	1753.8 (3)
Z	4
D_x (Mg m^{-3})	1.244
Radiation, wavelength (Å)	Mo $K\alpha$, λ = 0.71073
μ (mm^{-1})	0.091
$F(000)$ (e)	712
Crystal form	Platelet
Crystal size (mm)	0.3 × 0.2 × 0.02
Crystal colour	Colourless
Data collection	
Diffractometer	Stoe IPDS image-plate system
Data collection method	Oscillation scans
Absorption correction	None
No. of measured reflections	6256
No. of independent reflections	1443
No. of observed reflections	1443
Criterion for observed reflections	$I > 2\sigma(I)$
θ_{min}, θ_{max} (°)	2.37, 20.8
Range of h, k, l	$-5 \rightarrow h \rightarrow 5$ $-25 \rightarrow k \rightarrow 25$ $-11 \rightarrow l \rightarrow 11$
Refinement	
Refinement on	F^2
$R(F^2)$, $wR(F^2)$, S(all)	0.0469, 0.1364, 1.150
No. of reflections used in refinement	1443
No. of parameters used	246
H-atom treatment	Mixed
Weighting scheme	$w = 1/[\sigma^2(F_o^2) + (0.0908P)^2 + 0.0702P]$ where $P = (F_o^2 + 2F_c^2)/3$
$(\Delta/\sigma)_{max}$	0.001
$\Delta\rho_{min}$, $\Delta\rho_{max}$ (e Å^{-3})	−0.115, 0.168
Extinction method	None
Source of atomic scattering factors	*International Tables for Crystallography* (Vol. C, Tables 4.2.6.8 and 6.1.1.4)
Refined volume ratio	0.132 (2)
Correlation matrix elements larger than 0.85	
Between	Correlation
z(O1B)/y(O1A)	0.904
U^{23}(O3B)/z(O3B)	−0.890
z(O3B)/z(O3A)	−0.888
y(O1A)/occ(O)	−0.873
z(O3B)/U^{23}(O3A)	−0.861
U^{23}(O3B)/z(O3A)	0.851
Computer programs	
Data collection	*EXPOSE* (Stoe, 1997)
Cell refinement	*INDEX*, *CELL* (Stoe, 1997)
Data reduction	*PROFILE*, *EMS*, *INTEGRATE* (Stoe, 1997), *XPREP* (Siemens, 1996*b*), local programs
Structure solution	*SHELXS*97 (Sheldrick, 1997*b*)
Structure refinement	*SHELXL*97 (Sheldrick, 1997*a*)
Molecular graphics	*XP* (Siemens, 1996*a*)

$$\sigma^2(\kappa_{ij}) = \sum_{n=1}^{N}\left[\sigma^2(I_{i,n}) + \kappa_{ij}^2\sigma^2(I_{j,n})\right] \Big/ \left(\sum_{m=1}^{N} I_{j,m}\right)^2. \quad (6)$$

The twinning volume ratio, v_i, enters the structure-factor expression of a nonoverlapped reflection according to $F_{i,n}^2(\mathbf{H}) = v_i F_{0,n}^2(\mathbf{H})$, with $\sum_{i=1}^{D} v_i = 1$. Taking the ratio between $F_{i,n}^2$ and $F_{j,n}^2$, the scaling ratio becomes $\kappa_{ij} = v_i/v_j$. Summing over i gives

$$v_j = \left(\sum_{i=1}^{D} \kappa_{ij}\right)^{-1} \quad (7)$$

with $\kappa_{jj} = 1$. The associated square of the s.u. is

$$\sigma^2(v_j) = \sum_{i=1}^{D} \sigma^2(\kappa_{ij}) \Big/ \left(\sum_{m=1}^{D} \kappa_{mj}\right)^4, \quad (8)$$

where $\sigma^2(\kappa_{jj})$ is set to zero.

The present approach formalizes an intuitive method of estimating the volume ratios. It can be used for detwinning prior to structure solution, which can be helpful in cases where no structure solution can be obtained from the raw data. Further, it can assist in interpreting twinning phenomena in more complicated cases: two reflection classes can only originate from the same domain if the corresponding volume ratios are the same. This gives a necessary, though not sufficient, condition for the correctness of a specific interpretation of the diffraction pattern of twinned crystals.

We used this formalism to establish a direct estimation of the twinning ratio in phase III. The estimation was based on the space-group-averaged superstructure reflections present in both domains. This was the case for 208 out of the 212 superstructure reflections of domain 2. Using (5) and (7) gives v_2 = 0.139 (1). This is in very good agreement with the results of the refinement: v_2 = 0.132 (2) (see below). It is likely that the twinning volume ratio is specimen dependent; for the study of phase IV we used another specimen and, indeed, obtained a different volume ratio in phase IV (Birkedal *et al.*, 1999).

5. Data reduction, structure solution and refinement

The data were integrated in the supercell and split into three classes: common reflections, superstructure reflections from domain 1, and the much weaker superstructure reflections from domain 2. During the following data analysis, it became evident that the weak reflections were not properly integrated. This was apparent during the calculation of the intensity ratio

Table 3. *Fractional atomic coordinates and equivalent isotropic displacement parameters (Å^2)*

$U_{eq} = (1/3)\Sigma_i\Sigma_j U^{ij} a^i a^j \mathbf{a}_i.\mathbf{a}_j$; U_{iso} for H atoms.

	x	y	z	U_{eq}/U_{iso}	Occupancy
O1*A*	−0.025 (7)	0.875 (2)	0.098 (4)	0.108 (12)	0.29 (4)
O1*B*	−0.056 (2)	0.8552 (4)	0.0475 (16)	0.076 (3)	0.29 (4)
O2*A*	0.291 (7)	0.8681 (16)	0.048 (4)	0.090 (11)	0.71 (4)
O2*B*	0.310 (2)	0.8795 (6)	0.0680 (14)	0.075 (4)	0.71 (4)
H2O	0.3406	0.8557	0.1214	0.112	0.71 (4)
C11	0.0823 (9)	0.88405 (15)	0.0257 (4)	0.0509 (12)	
C12	0.0111 (8)	0.92394 (16)	−0.0675 (4)	0.0568 (13)	
C13	−0.2383 (8)	0.94317 (15)	−0.0946 (4)	0.0575 (13)	
C14	−0.3034 (9)	0.97712 (18)	−0.2026 (5)	0.0692 (15)	
C15	−0.5437 (8)	1.00182 (18)	−0.2334 (4)	0.0607 (12)	
C16	−0.6007 (9)	1.02870 (18)	−0.3506 (4)	0.0666 (15)	
C17	−0.8278 (9)	1.05880 (16)	−0.3857 (4)	0.0596 (14)	
C18	−0.8753 (8)	1.07994 (17)	−0.5081 (4)	0.0569 (13)	
C19	−1.0829 (9)	1.11470 (15)	−0.5487 (5)	0.0546 (12)	
O3*A*	−1.237 (8)	1.1182 (16)	−0.499 (5)	0.072 (9)	0.29 (4)
O4*A*	−1.119 (6)	1.1335 (18)	−0.652 (4)	0.078 (11)	0.29 (4)
O3*B*	−1.178 (4)	1.1367 (7)	−0.486 (2)	0.088 (5)	0.71 (4)
O4*B*	−1.130 (2)	1.1250 (7)	−0.6618 (14)	0.067 (4)	0.71 (4)
H4O	−1.2724	1.1373	−0.6868	0.101	0.71 (4)
N1	0.4557 (6)	0.79563 (12)	0.2069 (3)	0.0460 (9)	
H1	0.3891	0.823	0.1622	0.055	0.29 (4)
N2	0.4336 (6)	0.70364 (11)	0.2341 (3)	0.0449 (9)	
H2	0.3519	0.6746	0.2058	0.054	0.29 (4)
N3	0.8159 (6)	0.74534 (13)	0.2758 (3)	0.0495 (10)	
N4	0.5608 (7)	0.75981 (13)	0.4034 (3)	0.0509 (10)	
C1	0.3276 (8)	0.74864 (15)	0.1633 (4)	0.0486 (10)	
C2	0.7049 (7)	0.78895 (16)	0.2057 (4)	0.0507 (12)	
C3	0.4510 (9)	0.80276 (16)	0.3295 (4)	0.0566 (13)	
C4	0.6794 (8)	0.69955 (16)	0.2305 (4)	0.0548 (13)	
C5	0.8048 (8)	0.75397 (17)	0.3963 (5)	0.0589 (12)	
C6	0.4308 (7)	0.71313 (15)	0.3560 (4)	0.0483 (12)	

described above. Several outliers among the weakest reflections fell out of the linear relation described by the remaining data points. In addition, the initial stages of the refinement including all weak reflections showed poor convergence and the presence of several outliers. The outliers were all weak intensities. We conclude that the problem arose from the difficulties in the integration. This is especially damaging in the present case, because one domain is very much weaker than the other. Therefore, we chose to include in the further analysis only reflections that gave an averaged intensity with $I/\sigma(I) \geq 2$. For reflections common to both domains, 2766 out of 3821 intensities were kept. For superstructure reflections of domain 1, we retained 2543 out of 3839, while for superstructure reflections of domain 2, 947 out of 3871 were used. These reflection classes were averaged independently according to the space-group symmetry (see Table 1). The merging R value, R_{int}, for the superstructure reflections of domain 2 is very large since this reflection class is significantly weaker than the other two data classes, as shown by $\langle I/\sigma(I)\rangle$ in Table 1. This observation is in agreement with the observed twinning ratio calculated above. Experimental and refinement parameters are given in Table 2.

The structure was solved by direct methods (Sheldrick, 1997*b*) using common reflections and the superstructure reflections of domain 1. The solution gave positions for all heavy atoms. The structure was refined using all reflections fulfilling the aforementioned $I/\sigma(I) \geq 2$ criterion, employing the HKLF5 option in *SHELXL*97 (Sheldrick, 1997*a*), under which the twinning volume ratio is directly refined. All heavy atoms were refined anisotropically. For all methylene groups, H atoms were included in a riding model; each displacement parameter was fixed at 1.2 times the value of the equivalent isotropic displacement parameter of the C atom to which the H atom is bonded. The acid groups are disordered. They were modelled by splitting each O atom over two sites. The C—O distances showed that the structure is a superposition of a carboxylic acid (—COOH), for which the O atoms are identified by suffix *B*, and a carboxylate group (—COO$^-$), for which the O atoms are assigned suffix *A*. For the carboxylate groups, the corresponding H atoms are situated on N1 (H1) and N2 (H2) of the HMT molecules; they were included as riding atoms with U_{iso}(H) = 1.2U_{eq}(N). H atoms on the carboxylic acid groups where observed in the difference Fourier map and included in a riding model with U_{iso}(H) = 1.5U_{eq}(O). Occupancies of the disordered atoms were refined under the constraints occ(O1*A*) = occ(O2*A*) = occ(H1) = occ(O3*A*) = occ(O4*A*) = occ(H2), occ(O1*B*) = occ(O2*B*) =

Table 4. *Bond distances (Å) and angles (°) in the HMT molecule*

N1—C1	1.457 (5)	C1—N1—C2	108.3 (3)
N1—C2	1.482 (5)	C1—N1—C3	107.9 (3)
N1—C3	1.477 (6)	C3—N1—C2	108.3 (4)
N2—C1	1.477 (5)	C4—N2—C6	108.7 (3)
N2—C4	1.464 (5)	C4—N2—C1	107.9 (3)
N2—C6	1.475 (6)	C6—N2—C1	108.0 (3)
N3—C2	1.454 (6)	C2—N3—C4	108.3 (4)
N3—C4	1.457 (6)	C2—N3—C5	107.8 (3)
N3—C5	1.469 (7)	C4—N3—C5	108.4 (3)
N4—C3	1.459 (6)	C3—N4—C5	108.8 (3)
N4—C5	1.471 (6)	C3—N4—C6	108.0 (4)
N4—C6	1.464 (5)	C6—N4—C5	107.9 (3)
		N1—C1—N2	111.7 (3)
		N3—C2—N1	112.0 (3)
		N4—C3—N1	111.8 (3)
		N3—C4—N2	112.2 (3)
		N3—C5—N4	112.4 (3)
		N4—C6—N2	111.7 (3)

Table 5. *Bond distances (Å) and angles (°) in the acid molecule*

O1*A*—C11	1.22 (3)	O1*A*—C11—O2*A*	117 (2)
O2*A*—C11	1.25 (3)	O1*A*—C11—C12	124.2 (17)
O1*B*—C11	1.190 (11)	O2*A*—C11—C12	116.7 (17)
O2*B*—C11	1.298 (14)	O1*B*—C11—O2*B*	123.6 (9)
C11—C12	1.492 (6)	O1*B*—C11—C12	122.2 (7)
C12—C13	1.500 (6)	O2*B*—C11—C12	113.5 (8)
C13—C14	1.518 (7)	C11—C12—C13	116.7 (4)
C14—C15	1.505 (6)	C12—C13—C14	112.3 (4)
C15—C16	1.512 (6)	C15—C14—C13	117.1 (4)
C16—C17	1.507 (6)	C14—C15—C16	112.1 (4)
C17—C18	1.507 (6)	C17—C16—C15	116.7 (4)
C18—C19	1.490 (6)	C16—C17—C18	111.7 (4)
C19—O3*A*	1.22 (5)	C19—C18—C17	116.8 (4)
C19—O4*A*	1.29 (4)	O3*A*—C19—O4*A*	119 (3)
C19—O3*B*	1.20 (2)	O3*A*—C19—C18	123 (2)
C19—O4*B*	1.322 (15)	O4*A*—C19—C18	116.5 (14)
		O3*B*—C19—O4*B*	122.4 (13)
		O3*B*—C19—C18	124.9 (12)
		O4*B*—C19—C18	112.0 (8)

occ(H2O) = occ(O3*B*) = occ(O4*B*) = occ(H4O), and occ(O3*B*) = 1 − occ(O3*A*). In an initial refinement, the grouping O1, O2 was not constrained to have the same occupancies as O3, O4. However, the *R* values were the same, and the refined values agreed within 2 s.u.'s. Therefore, we employed the more constrained model in the final description. The O atoms were refined anisotropically with rigid-link restraints between the C and O. The final agreement factors are given in Table 2. The largest correlation matrix elements (see Table 2) are all between parameters of the disordered O atoms and not larger than 0.91. Coordinates of the refined atoms are given in Table 3.†

† Supplementary data for this paper are available from the IUCr electronic archives (Reference: SE0259). Services for accessing these data are described at the back of the journal.

Table 6. *Tosion angles (°) and angles (°) between acid-group planes in the acid molecule*

For the acid-group planes, the diagonal elements of the table give the r.m.s. deviation from planarity in Å. The planes are least-squares planes defined as: 1–2*A* = C12, C11, O1*A*, O2*A*; 1–2*B* = C12, C11, O1*B*, O2*B*; 3–4*A* = C18, C19, O3*A*, O4*A*; 3–4*B* = C18, C19, O3*B*, O4*B*; chain = C11, C12, C13, C14, C15, C16, C17, C18, C19.

C13—C12—C11—O1*A*	−18 (4)
C13—C12—C11—O2*A*	−180 (2)
C13—C12—C11—O1*B*	27.2 (12)
C13—C12—C11—O2*B*	−161.7 (9)
C11—C12—C13—C14	−171.1 (4)
C12—C13—C14—C15	−175.7 (4)
C13—C14—C15—C16	−172.3 (4)
C14—C15—C16—C17	−174.7 (4)
C15—C16—C17—C18	−175.1 (4)
C16—C17—C18—C19	−174.2 (4)
C17—C18—C19—O3*A*	−15 (3)
C17—C18—C19—O4*A*	179 (2)
C17—C18—C19—O3*B*	18.9 (16)
C17—C18—C19—O4*B*	−170.7 (10)

Acid-group planes

	1–2*A*	3–4*A*	1–2*B*	3–4*B*	Chain
1–2*A*	0.05	13 (4)	31 (3)	35 (3)	9 (3)
3–4*A*	–	0.039	43 (2)	22 (2)	5 (3)
1–2*B*	–	–	0.027	64.4 (9)	38.2 (6)
3–4*B*	–	–	–	0.028	26.4 (9)
Chain	–	–	–	–	0.094

Table 7. *Hydrogen-bonding geometry (Å, °)*

D—H···*A*	*D*—H	H···*A*	*D*···*A*	*D*—H···*A*
With molecule type *B*				
O2*B*—H2O···N1	0.87	1.89	2.730 (16)	162.9
O4*B*—H4O···N2^{i}	0.87	1.98	2.699 (14)	139.6
C2—H2*A*···O1*B*^{ii}	0.97	2.63	3.157 (14)	114.8
C3—H3*B*···O3*B*^{iii}	0.97	2.58	3.19 (2)	121.4
C5—H5*A*···O3*B*^{iv}	0.97	2.62	3.58 (2)	170.1
C5—H5*B*···O1*B*^{v}	0.97	2.4	3.345 (15)	163.2
C12—H12*A*···O4*B*^{vi}	0.97	2.74	3.706 (18)	176.3
With molecule type *A*				
N1—H1···O2*A*	0.91	1.76	2.65 (4)	165
N1—H1···O1*A*	0.91	2.71	3.46 (3)	139.9
N2—H2···O3*A*^{vii}	0.91	2.79	3.51 (5)	137.7
N2—H2···O4*A*^{vii}	0.91	1.72	2.59 (4)	160.4
C2—H2*B*···O1*A*^{ii}	0.97	2.62	3.21 (4)	119.7
C6—H6*B*···O2*A*^{viii}	0.97	2.74	3.38 (4)	124.4
C—H···N, common to *A* and *B*				
C2—H2*A*···N4^{ix}	0.97	2.79	3.682 (6)	153.5
C1—H1*B*···N3^{x}	0.97	2.74	3.622 (6)	151.8
C6—H6*A*···N3^{x}	0.97	2.68	3.580 (6)	154.1

Symmetry codes: (i) $-1-x, \frac{1}{2}+y, -\frac{1}{2}-z$; (ii) $1+x, y, z$; (iii) $-1-x, 2-y, -z$; (iv) $-x, 2-y, -z$; (v) $1+x, \frac{3}{2}-y, \frac{1}{2}+z$; (vi) $-1-x, 2-y, -1-z$; (vii) $-1-x, y-\frac{1}{2}, -\frac{1}{2}-z$; (viii) $x, \frac{3}{2}-y, \frac{1}{2}+z$; (ix) $x, \frac{3}{2}-y, z-\frac{1}{2}$; (x) $x-1, y, z$.

6. Description of the structure

The atom-labelling scheme is presented in Fig. 4. Bond distances and angles for the HMT molecule are given in Table 4. The geometry of the HMT molecule is as expected. As mentioned above, the acid groups are

disordered, O atoms with suffix *A* corresponding to carboxylate groups and O atoms with suffix *B* to carboxylic acid groups. The occupancies of the two carboxylate groups refine to practically the same values (Table 3). Therefore, we conclude that the chains adopt two forms: pure carboxylate, *AA*, and pure carboxylic acid, *BB*. The *BB* chain is the major form, the ratio between the two forms being 0.41:1. Table 5 gives bond lengths and angles for the acid molecule. The C—O distances in the carboxylate groups are, as expected, equal within 2 s.u.'s. For the carboxylic acid groups, the C—O and C═O distances also fall within expected ranges. This lends support to the established structural model. Torsion angles and information on the acid-group planes are given in Table 6. As seen from the root-mean-square (r.m.s.) deviations from planarity, all these groupings are planar, as expected. The 1–2*A* and 3–4*A* planes are very close to being in the chain plane. This is reflected in the torsion angles C13—C12—C11—O1*A*/O2*A* and C17—C18—C19—O3*A*/O4*A*, that are within at most 5 s.u.'s of 0 and ±180°. The maximum deviation from this plane is shown by C11 [−0.160 (4) Å] while the O atoms lie at distances of −0.23 (7), −0.02 (5), 0.05 (5) and −0.10 (5) Å, for O1*A*, O2*A*, O3*A* and O4*A*, respectively. For the *BB* molecule, the situation is different. The acid-group planes are turned by about 30° out of the chain plane. The distances from the chain plane are −0.932 (14), 0.351 (16), 0.614 (22) and −0.337 (21) Å for O1*B*, O2*B*, O3*B* and O4*B*, respectively. Note that O2*B* is on one side of the plane while O4*B* is on the other.

6.1. *Overall packing*

HMT generally only accepts two strong hydrogen bonds (Blažević *et al.*, 1979), *i.e.* only two N atoms are involved in strong hydrogen bonds, either as donors (here *AA* molecules) or as acceptors (here *BB* molecules). The topology of HMT leads then to a hydrogen-bonded wedge-shaped motif O1O2–chain–O3O4···HMT···O1O2–chain–O3O4, where the first chain is related to the second by the symmetry operation $-1-x, -\frac{1}{2}+y, -\frac{1}{2}-z$. The angle between the two chain planes in this unit is 70.25 (19)°. As the chains have two active ends, an infinite hydrogen-bonded zigzag chain along **b** is obtained (see Figs. 5 and 6). This motif has recently been found in several adducts of HMT with bisphenols (Coupar, Glidewell & Ferguson, 1997).

It is worth noting that HMT occasionally accepts more than two hydrogen bonds, in particular in adducts with trisphenols, where in the 1:1 adduct with 1,1,1-tris(4-hydroxyphenyl)ethane (Coupar, Ferguson *et al.*, 1997), the 1:2 (two HMT) adduct with 1,1,1-tris(4-hydroxyphenyl)ethane (Coupar, Glidewell & Ferguson, 1997) and the 2:3 (three HMT) adduct with 1,3,5-trihydroxybenzene (Coupar, Glidewell & Ferguson, 1997), HMT is an acceptor of three hydrogen bonds. The same is the case in HMT hexahydrate (Mak, 1965) and the 3:1 adduct of phenol and HMT (Jordan & Mak, 1970). To the best of our knowledge, these are all the existing cases of HMT acting as an acceptor of three hydrogen bonds.

The infinite zigzag chains pack on top of each other, creating a puckered plane coinciding with $(10\bar{2})$ as indexed in the cell of domain 1 (Fig. 6). From purely geometrical reasons, it can be expected that the intermolecular coherence within this plane is strong. Due to the shape of the packed zigzag chains, it is more difficult to displace molecules within this plane than perpendicular to it. This packing means that layers of only HMT and only acid molecules are created perpendicular to **b**. The acid chains thus form a herringbone-like arrangement, as shown in Figs. 5 and 6. Within an acid chain layer, the chain planes (spanned by the C atoms) are all coplanar. However, along **c**, neighbouring acid chains are related by a *c*-glide so that the motif is ..., O1O2–chain–O3O4, O3O4–chain–O1O2, O1O2–chain–O3O4, ... The *c*-glide relation also holds in an HMT layer.

6.2. *Details of packing – hydrogen bonding*

The packing is governed by hydrogen bonding. In Table 7, geometric characteristics of the different hydrogen bonds are given. Hydrogen bonds were located using the criteria H···*A* < 2.8 Å and *D*—H···*A* > 110°. Figs. 5, 6 and 7 show the packing and the intermolecular interactions. The hydrogen bonds were divided into two classes: hydrogen bonds with *D*···*A* < 2.5 Å and *D*—H···*A* > 130° belong to the first class, while the remaining, weaker, hydrogen bonds belong to the second class. In all figures showing hydrogen bonds,

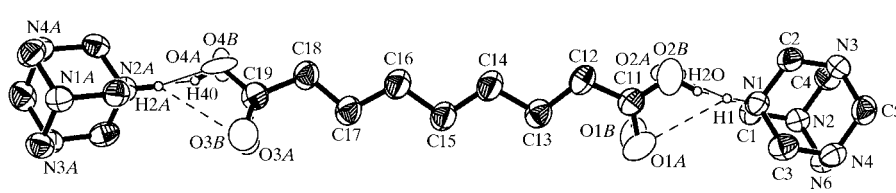

Fig. 4. Atomic labelling scheme with displacement ellipsoids drawn at the 50% probability level. The view is onto the least-squares plane of the acid-chain C atoms. C atoms are drawn with full displacement ellipsoids with shaded segments, N atoms with ellipsoid border and principal axes, while O atoms are drawn with ellipsoid borders only. HMT molecule *A* is generated by the symmetry operation $-1-x, \frac{1}{2}+y, -\frac{1}{2}-z$. Only refined H atoms are shown.

bonds belonging to the first class are drawn with thin solid lines, while the others are represented by dashed lines.

Since the packing of *AA* molecules is different from the packing of *BB* molecules, we now consider the two motifs in turn.

6.2.1. *BB molecules*. The primary intermolecular interactions of the *BB* molecules are the O—H···N interactions. The overall interaction scheme of both carboxylic acid groups is the same. However, small differences are present. Within the plane ($10\bar{2}$), both O—H···N interactions and two C—H···O interactions are found (see Fig. 6). The C—H···O bonds in ($10\bar{2}$) without doubt stabilize the structure and participate in determining the orientation of the acid groups. The two short-distance small-angle interactions (C2—H2*A*···O1*B* and C3—H3*B*···O3*B*) might be forced contacts generated by the geometry imposed by the O—H···N and C5—H5*A*/*B*···O3*B*/1*B* interactions. It is an open question at which geometry C—H···O contacts change from being attractive to being forced and therefore repulsive (Jeffrey, 1997, pp. 96–97). The chain–chain interaction C12—H12*A*···O4*B* is probably slightly attractive in nature and helps to stabilize the structure. It links the ($10\bar{2}$) layers approximately along **c**.

The fact that the *BB* molecules form the major component leads to the conclusion that this packing motif is more stable than that of the *AA* molecules. If it is assumed that the occupation ratio originates from the difference in energy between the two motifs, the energy difference can be estimated from $\Delta E = RT \ln[\mathrm{occ}(AA)/\mathrm{occ}(BB)]$ giving $\Delta E \simeq -2$ kJ mol^{-1}.

6.2.2. *AA molecules*. O2*A* and O4*A* of the carboxylate groups are hydrogen bonded to N1 and N2, respectively, with geometries typical for N—H^{+}···O hydrogen bonds (Jeffrey, 1997). The bonding situation can be considered as a three-centre hydrogen bond. The difference between the long and the short bond, Δ(N···O), is 0.81 Å for O1*A*, O2*A* and 0.92 Å for O3*A*, O4*A*.† It is worth noting that the long and short distances are very similar to the corresponding distances in several amino-acid crystal structures (Jeffrey, 1997, p. 69). The carboxylate groups are turned to accommodate the three-centre bonds so that the C—H···O contacts with C5 are no longer possible (see Figs. 5 and 6). Thus the ($10\bar{2}$) layer is no longer stabilized by C—H···O contacts. The rotation of the carboxylates also removes the inter-chain C—H···O bond present in the *BB* packing. The nature of the two aforementioned C—H···O contacts present in the *AA* packing is undecidable; the attractiveness of the interaction cannot be asserted with confidence – they might be repulsive. One can tentatively conclude that it is the lack of stabilizing C—H···O contacts that makes the *AA* packing less stable than the *BB*. This should be further investigated either experimentally or *via* theoretical calculations before any definite conclusion can be made.

6.2.3. *The HMT layer*. The HMT layer (Fig. 7) resembles the (110) layer of pure HMT (Kampermann *et al.*, 1995). In pure HMT, each N atom in this layer accepts three equivalent C—H···N interactions with geometries H···N = 2.82, C···N = 3.81 Å and C—H···N = 152.1° at 200 K. In phase III, the cages are tilted so that N3 accepts two C—H···N interactions, while N4 accepts only one. They have the same angles, but the C···N distances are shorter than in pure HMT.

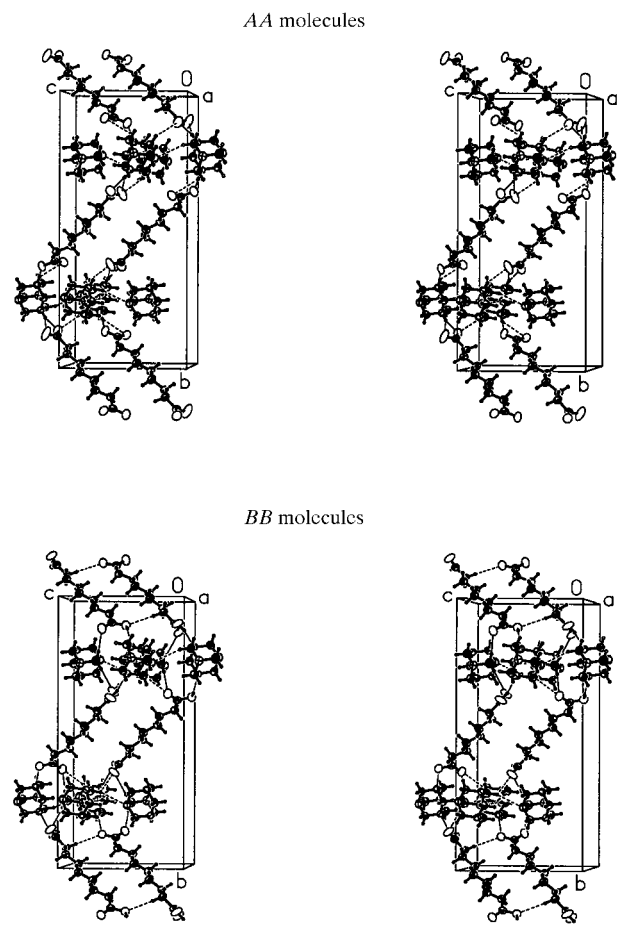

Fig. 5. Stereoview of the packing of *AA* (top) and *BB* molecules (bottom). All intermolecular interactions are shown. Displacement ellipsoids are plotted at the 50% probability level; atoms are drawn as in Fig. 4.

† The sum of the two N—H···O angles and O···H···O is 346° for N1, H1, O1*A*, O2*A*, and 336° for N2, H2, O3*A*, O4*A*. Following one definition of three-centre hydrogen bonds, these angles should be close to 360° (Jeffrey, 1997, p. 22). Using another definition, the H atoms should be within 0.2 Å of the N–O1–O2 plane (Jeffrey, 1997, p. 22); here we find 0.10 Å for H1 and −0.17 Å for H2. Considering these observations, one could question the existence of a three-centre bond. However, the uncertainties in the cited angles are large, as the s.u.'s of the positions of the *A* O atoms are large. Therefore, we accept these hydrogen bonds as three-centred.

6.3. *Comparison with phase II – doubling of* **c**

The overall packing of phase II (Gardon *et al.*, 1999) is the same as that of phase III: in both phases a herringbone arrangement of chains separated by sheets of HMT is observed. The main difference consists of the ordering of the chain planes and the tilt of the cages thereby induced.

Consider Fig. 7. The tilt of the HMT molecules out of the **ac** plane can be defined as the angle between the planes through C1, C5, N3 and N4 in two neighbouring molecules. This gives a tilt of 18.39 (6)°. In phase II the HMT molecules are related by translation and no tilt is observed. The tilt is linked to the alternation of chain conformations along **c**. It is the cage tilt/chain alternation that induces the doubling of **c**. The tilt is due to the combination of O—H···N and C—H···O interactions in $(10\bar{2})$. The detailed energetics of the ordering cannot

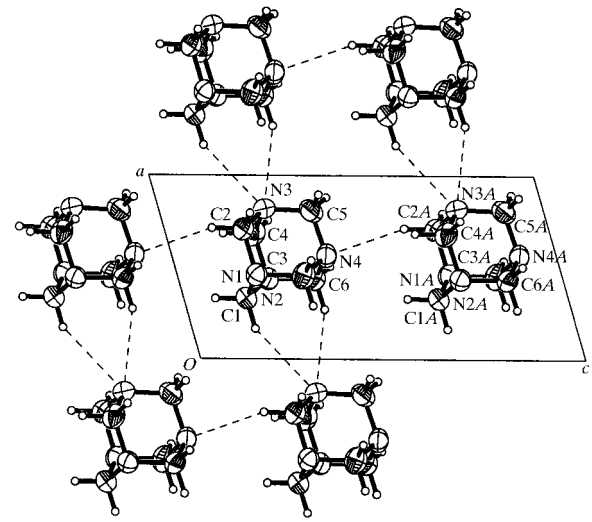

Fig. 7. Projection along **b** onto a layer of HMT showing the C—H···N interactions and the tilt of the HMT molecules with respect to the **ac** plane. The symmetry operation linking the two molecules within the cell is $x, \frac{3}{2} - y, \frac{1}{2} + z$. Displacement ellipsoids are plotted at the 50% probability level; atoms are drawn as in Fig. 4.

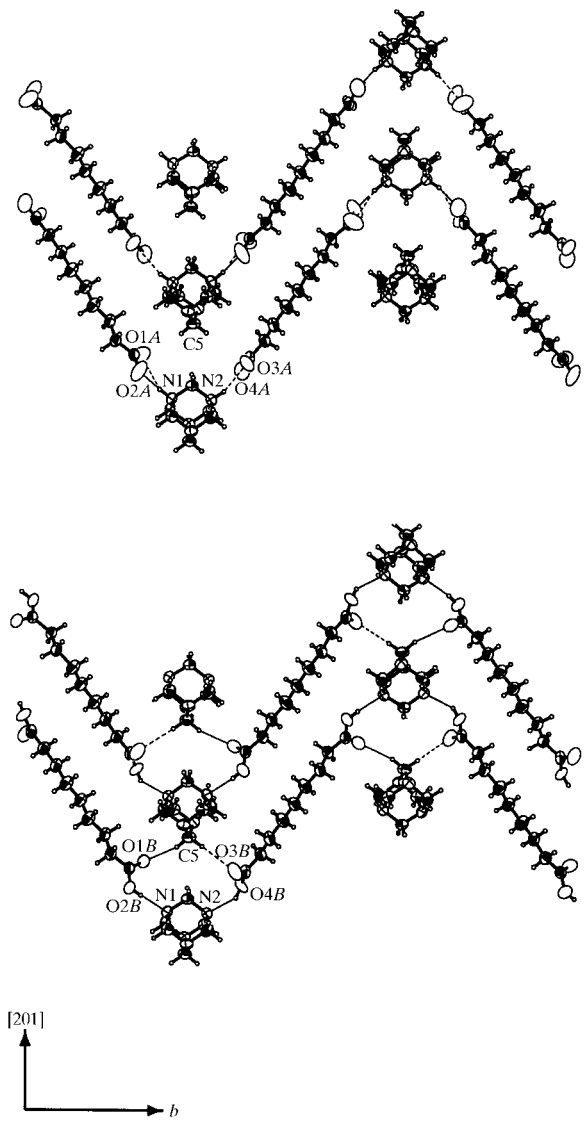

Fig. 6. Perspective view of one layer of the structure onto the plane $(10\bar{2})$ for *AA* (top) and *BB* molecules (bottom). Displacement ellipsoids are plotted at the 50% probability level; atoms are drawn as in Fig. 4.

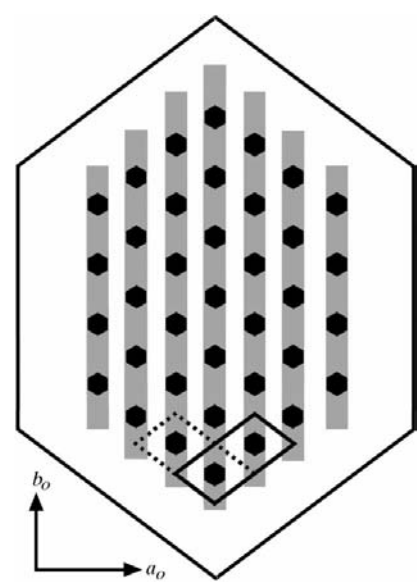

Fig. 8. Schematic view of a twinned crystal showing strongly correlated directions and thereby the reason why only two domain types are observed. Hexagons mark the positions of the HMT molecules. Planes of strong correlation are indicated by a set of hexagons contained within a grey rectangle. Unit cells of domain 1, thin solid lines, and domain 2, thin dashed lines, are indicated. The unit-cell axes indicated at the bottom left are those of the orthorhombic system of phase II.

be unambiguously assigned to either the O—H···N or the C—H···O interactions from purely structural studies. Note that the combination of these interactions occurs only in the major component, the *BB* molecules. A detailed comparison of the three crystalline phases of HMTA will be presented in a forthcoming paper discussing phase IV (Birkedal *et al*., 1999).

7. Conclusions

We have studied the II→III phase transition in the 1:1 adduct of hexamethylenetetramine and azelaic acid. The transition, going from *Cmcm* to $P2_1/c$, produces a doubling of the volume of the primitive diamond-shaped cell of phase II. The system was identified as TLQS twinned and a structural model was refined from the complete set of data. During the phase transition, the chain planes order. Two chain conformations alternate along the doubled cell parameter. The acid groups remain disordered.

Phase II of HMTA exhibits diffuse rods at room temperature. On these rods emerge a set of Bragg superstructure reflections in phase III. This phenomenon was previously interpreted as a change in the correlation length during the phase transition (Gardon *et al*., 1999). Now it is possible to give more details about the mechanisms driving the transition. The stabilization is induced by a combination of O—H···N and C—H···O interactions. At the phase transition, the geometrical constraints imposed by these interactions become more important than the thermal energy, and the orientational freedom of the aliphatic chain is reduced. This leads to the enlargement of the correlation length in the plane $(10\bar{2})$.

As discussed above, four single-domain states are allowed: two from the mirror planes lost in the transition, and two from the doubling of the unit cell. Domain walls of the latter are not observable with the methods used in this study since the corresponding domains have the same orientation of the lattice and the optical indicatrix. Domain walls of the former could be parallel to either of the lost mirror planes. However, only domain walls parallel to $(10\bar{2})$ are observed. The reason for this can be understood by considering the directions of strong intermolecular correlation. Fig. 8 presents a schematic view of a crystal. HMT molecules are shown as black hexagons and the strongly correlated $(10\bar{2})$ planes are indicated. The orthorhombic axes, $\mathbf{a}_o$ and $\mathbf{b}_o$, are perpendicular and parallel, respectively, to $(10\bar{2})$. The mirror planes lost in the transition are perpendicular to $\mathbf{a}_o$ and $\mathbf{b}_o$. Therefore the $(10\bar{2})$ planes of two domains are parallel. The direction of strong correlation is the same for the two domains. Domain walls perpendicular to these strongly correlated planes are clearly energetically disfavoured. This explains why only domain walls parallel to $(10\bar{2})$ are observed. The lamellar twinning can be interpreted as follows: at the phase transition, the structural changes take place at multiple sites in the crystal. The growth of the domains is faster parallel to $(10\bar{2})$ than perpendicular to this plane. This is in accordance with the observation of diffuse scattering in phase II, where domain precursors already exist.

Dr H. D. Flack is thanked for valuable discussions. Dr K. J. Schenk is thanked for practical help and many valuable discussions. HB gratefully acknowledges a grant from the Danish Research Academy.

References

Aizu, K. (1970). *Phys. Rev. B*, **2**, 754–772.
Birkedal, H., Gardon, M., Hostettler, M., Schwarzenbach, D., Chapuis, G. & Bonin, M. (1999). In preparation.
Blažević, N., Kolbah, D., Belin, B., Šunjić, V. & Kajfež, F. (1979). *Synthesis*, pp. 161–176.
Bonin, M. & Gardon, M. (1999). In preparation.
Bussien Gaillard, V., Chapuis, G., Dusek, M. & Petříček, V. (1998). *Acta Cryst.* A**54**, 31–43.
Bussien Gaillard, V., Paciorek, W., Schenk, K. & Chapuis, G. (1996). *Acta Cryst.* B**52**, 1036–1047.
Coupar, P. I., Ferguson, G., Glidewell, C. & Meehan, P. R. (1997). *Acta Cryst.* C**53**, 1978–1980.
Coupar, P. I., Glidewell, C. & Ferguson, G. (1997). *Acta Cryst.* B**53**, 521–533.
Gardon, M., Hostettler, M., Birkedal, H., Chapuis, G. & Bonin, M. (1999). In preparation.
Giacovazzo, C. (1992). *Fundamentals of Crystallography* ch. 2, pp. 83–87. International Union of Crystallography/Oxford University Press.
Hamilton, W. C., Rollet, J. S. & Sparks, R. A. (1965). *Acta Cryst.* **18**, 129–130.
Jameson, G. B. (1982). *Acta Cryst.* A**38**, 817–820.
Jeffrey, G. A. (1997). *An Introduction to Hydrogen Bonding.* Oxford University Press.
Jordan, T. H. & Mak, T. C. W. (1970). *J. Chem. Phys.* **52**, 3790–3794.
Kampermann, S. P., Sabine, T. M., Craven, B. M. & McMullan, R. K. (1995). *Acta Cryst.* A**51**, 489–497.
Mak, T. C. W. (1965). *J. Chem. Phys.* **43**, 2799–2805.
Sheldrick, G. M. (1997*a*). *SHELXL*97. *Program for the Refinement of Crystal Structures.* University of Göttingen, Germany.
Sheldrick, G. M. (1997*b*). *SHELXS*97. *Program for the Solution of Crystal Structures.* University of Göttingen, Germany.
Siemens (1996*a*). *XP*. Version 5.04. Siemens Analytical X-ray Instruments Inc., Madison, Wisconsin, USA.
Siemens (1996*b*). *XPREP*. Version 5.04. Siemens Analytical X-ray Instruments Inc., Madison, Wisconsin, USA.
Sparks, R. A. (1970). *Crystallographic Computing*, edited by F. R. Ahmed, S. R. Hall & C. P. Huber, pp. 182–184. Copenhagen: Munksgaard.
Stoe (1997). *IPDS 2.87 Software Manual.* Stoe and Cie, Darmstadt, Germany.
Wadhawan, V. K. (1997). *Acta Cryst.* A**53**, 546–555.